Monthly Notices of the ROYAL ASTRONOMICAL SOCIETY

MNRAS **513,** 5780–5789 (2022) https://doi.org/10.1093/mnras/stac1283
Advance Access publication 2022 May 10

Modelling the formation of the first two neutron star–black hole mergers, GW200105 and GW200115: metallicity, chirp masses, and merger remnant spins

Debatri Chattopadhyay [1,2,3]★ Simon Stevenson [1,2] Floor Broekgaarden [4] Fabio Antonini [3] and Krzysztof Belczynski[5]

[1]*Centre for Astrophysics and Supercomputing, Swinburne University of Technology, John Street, Hawthorn, Victoria 3122, Australia*
[2]*The ARC Centre of Excellence for Gravitational Wave Discovery, OzGrav, Melbourne, Victoria 3122, Australia*
[3]*School of Physics and Astronomy, Gravity Exploration Institute, Cardiff University, Cardiff CF24 3AA, UK*
[4]*Center for Astrophysics | Harvard & Smithsonian, 60 Garden Street, Cambridge, MA 02138, USA*
[5]*Nicolaus Copernicus Astronomical Center, Polish Academy of Sciences, ul. Bartycka 18, PL-00-716 Warsaw, Poland*

Accepted 2022 May 5. Received 2022 May 5; in original form 2022 March 11

ABSTRACT

The two neutron star–black hole mergers (GW200105 and GW200115) observed in gravitational waves by advanced LIGO and Virgo, mark the first ever discovery of such binaries in nature. We study these two neutron star–black hole systems through isolated binary evolution, using a grid of population synthesis models. Using both mass and spin observations (chirp mass, effective spin, and remnant spin) of the binaries, we probe their different possible formation channels in different metallicity environments. Our models only support LIGO data when assuming the black hole is non-spinning. Our results show a strong preference that GW200105 and GW200115 formed from stars with sub-solar metallicities $Z \lesssim 0.005$. Only two metal-rich ($Z = 0.02$) models are in agreement with GW200115. We also find that chirp mass and remnant spins jointly aid in constraining the models, while the effective spin parameter does not add any further information. We also present the observable (i.e. post-selection effects) median values of spin and mass distribution from all our models, which may be used as a reference for future mergers. Further, we show that the remnant spin parameter distribution exhibits distinguishable features in different neutron star–black hole sub-populations. We find that non-spinning, first born black holes dominate significantly the merging neutron star–black hole population, ensuring electromagnetic counterparts to such mergers a rare affair.

Key words: gravitational waves – black hole - neutron star mergers – stars: black holes – transients: tidal disruption events.

1 INTRODUCTION

The discovery of the two merger events GW200105 and GW200115 by the Advanced LIGO (Aasi et al. 2015) and Virgo (Acernese et al. 2015) gravitational-wave (GW) detectors marks the first observations of a black hole–neutron star (NS + BH) binary (Abbott et al. 2021). While there have been predictions of NS + BH systems before – accounting for their non-detection as well as future possibilities of detection (Sigurdsson 2003; Clausen, Sigurdsson & Chernoff 2014; Broekgaarden et al. 2021a; Chattopadhyay et al. 2021) – these two events provide the perfect opportunity to re-assess our understanding of the formation and evolution of massive binaries towards NS + BH systems.

The properties of GW200105 and GW200115 are consistent with astrophysical expectations for NS + BH binaries. Under a conservative prior allowing for large spins (<0.99) for the putative neutron star (NS), GW200105 is formed through the merger of a $8.9^{+1.2}_{-1.5}\,M_\odot$[1] black hole (BH) with a $1.9^{+0.3}_{-0.2}\,M_\odot$ NS, while GW200115 was through the merger of $5.7^{+1.8}_{-2.1}\,M_\odot$ BH with a $1.5^{+0.7}_{-0.3}\,M_\odot$ NS. Under a more constraining spin prior with low NS spins (<0.05), informed by observations of Galactic NSs, GW200105 and GW200115 are inferred to have formed through the coalescences of $8.9^{+1.2}_{-1.5}\,M_\odot$ BH with a $1.9^{+0.2}_{-0.2}\,M_\odot$ NS and $5.9^{+1.4}_{-2.1}\,M_\odot$ BH with a $1.4^{+0.6}_{-0.2}\,M_\odot$ NS, respectively. The effective spin ($\chi_{\rm eff}$) for GW200105 is found to be $-0.01^{+0.11}_{-0.15}$ ($-0.01^{+0.08}_{-0.12}$), while for GW200115 it is $-0.19^{+0.23}_{-0.35}$ ($-0.14^{+0.17}_{-0.34}$) for high (low) secondary spin priors, respectively. The mass and spin ($\chi_{\rm rem}$) of the post-merger remnant BH for GW200115 are obtained to be $10.4^{+2.7}_{-2.0}\,M_\odot$ and $0.43^{+0.04}_{-0.03}$, respectively. For GW200105, the remnant BH mass is $7.8^{+1.4}_{-1.6}\,M_\odot$ and $\chi_{\rm rem} = 0.38^{+0.04}_{-0.02}$. Rather than individual masses, mass ratio or individual spins, the chirp mass, effective and remnant spins are better constrained observable quantities.

The two NS + BH GW observations inspire us to ask some fundamental questions about their formation scenario. Broekgaarden & Berger (2021) have shown that the masses and merger rates inferred from GW200105 and GW200115 are consistent with formation through isolated binary evolution. In particular, they explored a large set of binary evolution models, and found that low kick velocities or relatively high common envelope (CE) efficiencies are preferred to simultaneously match the properties of double NS and double BH

★ E-mail: chattopadhyayd@cardiff.ac.uk
[1]90 per cent credible interval, from Abbott et al. (2021).

systems. In this study, we perform population synthesis simulations to investigate the birth order of the two types of compact objects – NS and BH – in the NS + BH systems, their masses, spins, and expected merger rates.

Particularly, we address the following primary questions in this study:

(a) Can the observational mass and spin signatures aid in distinguishing which sub-population – if the BH is born first (BHNS) or the NS is born first (NSBH)[2] – GW200105 and GW200115 were a part of?
(b) What are the overall predicted rates of BHNS versus NSBH formation across different metallicities?
(c) Did the pre-merger BHs for both the observations have a considerable spin ($\chi_{\rm BH} > 0.1$)?
(d) Does the observed remnant BH spins of GW200105 and GW200115 add information that can help constrain population synthesis models?
(e) Can the formation metallicity of the two NS + BH merger signals be inferred from the qualitative analysis of the observations?

In this paper, we use similar models to Broekgaarden & Berger (2021), but also compare measurements of the compact objects' spins to those predicted from our model. We assume first born BH to be non-spinning in all models and explore submodels in which the second born BH can either be spinning or non-spinning. For all but one of our models we assume that the spins of the component BHs are aligned with the binary orbital angular momentum prior to merger. We additionally test if spin misalignment due to supernova kicks heavily impacts our results. Using this additional information, we aim to constrain whether the NS or BH formed first in GW200105 and GW200115, and if we can place constraints on the metallicity of the environment in which they were born. We find in our study that though we cannot draw any additional constraints on binary evolution models, we do get an idea of the possible formation metallicities of these binaries through the analysis of the remnant spin in addition to chirp mass.

This paper is structured as follows: in Section 2, we outline the population synthesis methods we use to evolve isolated binaries; in Section 3, we discuss the results of our models by comparing them to the chirp mass and remnant spin observations of GW200105 and GW200115; in Section 4, we conclude and discuss our findings (including the answers to the five key questions outlined above) and their implications.

2 METHODS

In this paper, we study the possible formation of the two NS + BH observations through isolated binary evolution, using the population synthesis code COMPAS (Stevenson et al. 2017; Vigna-Gómez et al. 2018; Team COMPAS et al. 2022). COMPAS is based on updated stellar and binary evolution prescriptions from Hurley, Pols & Tout (2000) and Hurley, Tout & Pols (2002), respectively. There are many uncertainties in massive binary evolution (see e.g. Giacobbo, Mapelli & Spera 2018; Klencki et al. 2018; Broekgaarden et al. 2021a; Chattopadhyay et al. 2021; Belczynski et al. 2022). To investigate what we can learn from GW200105 and GW200115, we have produced a set of four main models ('Pessimistic', 'Optimistic', 'Kick_100', 'Alpha_2') with different stellar/binary evolution assumptions. 'Pessimistic' is our base model, with one key assumption about binary or stellar evolution varied in each of the following three models. In our choice of parameters for the models, we are guided by Fiducial/Default models of previous population synthesis studies (Stevenson et al. 2017; Vigna-Gómez et al. 2018; Neijssel et al. 2019; Chattopadhyay et al. 2020, 2021; Broekgaarden et al. 2021a). Based on the recent results from Broekgaarden & Berger (2021), we place particular emphasis on the importance of NS natal kicks, and the efficiency of the CE phase of binary evolution. Broekgaarden & Berger (2021) showed that natal kick velocities less than 100 km s^{-1} or high CE efficiency parameter ($\alpha_{\rm CE} \gtrsim 2$) provide good match to the merger rates of double BH, double NS and NS + BH inferred from GW observations (The LIGO Scientific Collaboration, the Virgo Collaboration & the KAGRA Collaboration 2021). Many processes in binary evolution are sensitive to metallicity. To examine the impact of metallicity (and to attempt to constrain the formation metallicities of GW200105 and GW200115), we evolve each of the four models at four different metallicities (Z). From lower to higher metallicity, we have models M-005 ($Z = 0.0005$), M-01 ($Z = 0.001$), M-05 ($Z = 0.005$), M-2 ($Z = 0.02$).

The zero-age main-sequence (ZAMS) mass of the primary (initially more massive) star is drawn from an initial mass function (Kroupa 2001), while the mass of the secondary is determined by drawing the mass ratio of the binary following an uniform distribution (Sana et al. 2012). All binaries at assumed to have a circular orbit at ZAMS (Hurley et al. 2002) The initial semimajor axes of the binaries follow the Sana et al. (2012) distribution, with the minimum and maximum of the distribution[3] being 0.1–1000 au, respectively. Variations in the distributions chosen for the initial conditions do not typically have a large impact on results for NS + BH binaries (e.g. de Mink & Belczynski 2015).

In the dominant channel of NS + BH formation, during Roche lobe overflow (RLOF), the mass transfer efficiency $\beta_{\rm MT}$, which is the ratio of mass accreted by the accretor and the mass lost by the donor is given by

$$\beta_{\rm MT} = \min\left(1, 10\frac{\tau_{\rm acc}}{\tau_{\rm don}}\right), \quad (1)$$

(Hurley et al. 2002; Schneider et al. 2015), where the thermal (Kelvin–Helmholtz) time-scales for the accretor and donor are denoted by $\tau_{\rm acc}$ and $\tau_{\rm don}$, respectively (see Chattopadhyay et al. 2021, equation 2 for further details). Mass accretion on to a compact object is assumed to be Eddington limited (Stevenson et al. 2017; Chattopadhyay et al. 2020).

The CE phase that may arise from unstable mass transfer is assumed to have $\alpha_{\rm CE} = 1$, where $\alpha_{\rm CE}$ denotes the fraction of the orbital energy available to unbind the envelope. The binding energy of the envelope is determined using the fits to detailed models from Xu & Li (2010). For model 'Alpha_2', we varied this efficiency parameter to $\alpha_{\rm CE} = 2$.

We assume the 'pessimistic' scenario for CE evolution, where a Hertzsprung gap (HG) donor is not allowed to survive CE and instead merges (Belczynski et al. 2007). In the 'Optimistic' model we alter this assumption, allowing for the possibility for HG donors to survive CE evolution and successfully eject the envelope. For all models, a

[2]NSBH systems are exciting especially as multimessenger sources – they can harbour recycled pulsars (Chattopadhyay et al. 2021) as the NSs is born first and NSBHs with high pre-merger BH spins have the possibility to produce exciting electromagnetic signatures at their mergers (Hu et al. 2022).

[3]The orbital period p in days is given by $f(\log p) \propto (\log p)^{\pi}$, where $\pi = -0.55$. The semimajor axis is calculated from p by using Kepler's third law for circular orbits.

NS companion is allowed to accrete during CE following MacLeod & Ramirez-Ruiz (2015), as described in details in Chattopadhyay et al. (2020). Since Pessimistic, Kick_100, and Alpha_2 are all under the 'pessimistic' CE framework, in this paper we sometimes refer to all three as 'pessimistic'.

For a more comprehensive description of COMPAS prescriptions of mass transfer during RLOF and CE, see the COMPAS methods paper (Team COMPAS et al. 2022), and specifically for the case of NS + BH we refer to Chattopadhyay et al. (2021), Broekgaarden et al. (2021a), and Broekgaarden & Berger (2021).

In COMPAS, we assume a Maxwellian supernova natal kick distribution for NSs, with the one-dimensional root mean square $\sigma_{\rm CCSN} = 265\,{\rm km\,s^{-1}}$ for core-collapse supernovae (Hobbs et al. 2005), $\sigma_{\rm ECSN} = \sigma_{\rm USSN} = 30\,{\rm km\,s^{-1}}$ for electron capture and ultrastripped supernovae (Podsiadlowski et al. 2004; Gessner & Janka 2018; Müller et al. 2019). The assumption for kick velocity is varied in model 'Kick_100', where $\sigma_{\rm CCSN}$ is assumed to be $100\,{\rm km\,s^{-1}}$. The BH natal kicks are also drawn from identical distributions as NS, but are scaled down by the fallback mass fraction (Fryer et al. 2012).

NSs are also treated as pulsars in COMPAS, with spins and surface magnetic fields computed in isolated (no mass transfer) and mass transfer (during RLOF and CE) cases, as detailed in Chattopadhyay et al. (2020). Natal spins of the NSs are drawn from an uniform distribution (between 10 and 100 ms) and they are expected to spin-down rapidly $\sim \mathcal{O}$(10–100 Myr). Angular momentum transfer during mass accretion can spin pulsars up as well. Chattopadhyay et al. (2021) estimated that the mass-weighted spin $\chi_{\rm NS} \lesssim 0.3$ for solar metallicity.

Due to efficient angular momentum transfer from the core to the envelope of BH progenitors, first born BHs are assumed to be non-spinning in all our models (Fuller & Ma 2019). The progenitor of the second born BH, however, may get spun up through tidal interaction with its compact object companion (in the case of this paper, a NS), depending on the orbital configuration of the binary (Qin et al. 2018; Bavera et al. 2020; Chattopadhyay et al. 2021; Hu et al. 2022). We assume two models – (i) BH-Q: where the second born BH is allowed to be spun up as guided through prescriptions for different metallicities from Qin et al. (2018) and (ii) BH-Z: where BHs produced through second supernovae are also non-spinning. While Chattopadhyay et al. (2021) focused on the pre-merger BH spin analysis of only solar metallicity $Z = 0.0142$ (Asplund et al. 2009) models (in that paper, we were more interested in the Galactic population), in this paper we explore a grid of four metallicities ($Z = 0.02, 0.005, 0.001, 0.0005$). For BH-Q models, the pre-merger, second-born BH spin $\chi_{\rm BH}$ is given as

$$\chi_{\rm BH} = \begin{cases} 0, & \text{for } \log_{10} P_{\rm orb} > x_1 \\ 1, & \text{for } \log_{10} P_{\rm orb} < x_2 \\ m \log_{10} P_{\rm orb} + c, & \text{for } x_2 \leq \log_{10} P_{\rm orb} \leq x_1 \end{cases}, \tag{2}$$

where

$$x_1; x_2; m; c = \begin{cases} 0.5; -0.5; -0.87; 0.57; & \text{for } Z = 0.02 \\ 0.5; -0.5; -0.70; 0.54; & \text{for } Z = 0.005 \\ 0.5; -0.5; -0.70; 0.54; & \text{for } Z = 0.001 \\ 0.3; -0.5; -1.02; 0.63; & \text{for } Z = 0.0005 \end{cases} \tag{3}$$

for different metallicities (using fits from Qin et al. (2018)).

We compute the effective spin parameter $\chi_{\rm eff}$ assuming that the spin of the NS ($\chi_{\rm NS}$) and the spin of the BH ($\chi_{\rm BH}$) are both completely aligned with the orbital angular momentum.

This might be the case if binary evolution processes such as tides and mass accretion (including during CE will have aligned the spins of the stars in the binary with the orbit, prior to the formation of the compact objects. Small kicks associated with the formation of the compact objects that do not disrupt the binary would not be expected to reintroduce significant misalignments (Stevenson et al. 2017).[4] The effective spin

$$\chi_{\rm eff} = \frac{m_{\rm BH}\chi_{\rm BH}\cos\theta_{\rm BH} + m_{\rm NS}\chi_{\rm NS}\cos\theta_{\rm NS}}{m_{\rm BH} + m_{\rm NS}} \tag{4}$$

from Cutler et al. (1993), where the misalignment angles $\theta_{\rm BH}$ and $\theta_{\rm NS}$ are both zero for all four COMPAS models.

To check if supernovae kicks can create significant misalignment in the binaries to account for a negative effective spin, we separately analyse a Pessimistic model simulated with StarTrack (Belczynski et al. 2005) – called 'PessimisticST' – as a special sanity check run – that also tracks the binary spin misalignment. PessimisticST allow inefficient tidal interaction that may not completely align the systems with respect to orbital angular momentum at the time of merger (see Olejak, Belczynski & Ivanova 2021 for details). Since StarTrack does not yet compute the spin evolution of NSs, the pre-merger $\chi_{\rm NS}$ was taken as 0.01 for all systems (guided by fig. 21 of Chattopadhyay et al. 2021). Although accounting for misalignment due to supernovae kicks, this model does not change our final conclusions.

The remnant BHs formed in NS + BH binary mergers are expected to be spinning. Qualitatively, the post-merger remnant spin depends on the mass ratio of the binary prior to merger, the spin of the BH and the NS quadrupole tidal polarizability Λ (Zappa et al. 2019). The latter is a function of NS compactness which depends on the equation of state of the NS (Damour & Nagar 2010; Hinderer et al. 2010), and hence its mass–radius relation. The primary contribution to the remnant BH spin is from the orbital angular momentum of the binary, which is determined by the mass ratio of the binary.

It is expected the NS would usually be either severely deformed or destructed due to tidal disruption in a few orbits before merger, or can also merger head-on with the BH if the innermost stable orbit is located within the radius of the BH (Lattimer & Schramm 1976; Hinderer et al. 2010; Foucart 2020). Current numerical models assume a non-spinning pre-merger NS and this assumption, though not correct, is still expected to produce reasonable results (Kochanek 1992; Zappa et al. 2019).

If the mass ratio of the NS + BH binary is $q_{\rm s} = M_{\rm BH}/M_{\rm NS}$ and its symmetric mass ratio is $\gamma = q_{\rm s}/(1+q_{\rm s})^2$, using fits from Zappa et al. (2019) we obtain the remnant BH spin

$$\chi_{\rm rem} = a_4 \times \gamma^4 + a_3 \times \gamma^3 + a_2 \times \gamma^2 + a_1 \times \gamma^1 + a_0, \tag{5}$$

where

$$\begin{aligned} a_4 &= -2310.4 \times \chi_{\rm BH}^2 + 2088.4 \times \chi_{\rm BH} - 400, \\ a_3 &= 1582.08 \times \chi_{\rm BH}^2 - 1417.68 \times \chi_{\rm BH} + 253.33, \\ a_2 &= -367.46 \times \chi_{\rm BH}^2 + 325.37 \times \chi_{\rm BH} - 54.99, \\ a_1 &= 34.43 \times \chi_{\rm BH}^2 - 32.83 \times \chi_{\rm BH} + 7.56, \\ a_0 &= -1.17 \times \chi_{\rm BH}^2 + 1.95 \times \chi_{\rm BH} - 0.1, \end{aligned} \tag{6}$$

as was determined in Chattopadhyay et al. (2021), under the assumption of a constant Λ for all NSs, appropriate given that we assume all NSs have a radius of 12 km.

We noticed in our analysis that although there were instances of models deemed as accepted/potential match by $\chi_{\rm eff}$ (solely or jointly

[4]There can be infrequent cases of mass transfer anti-aligning the spin of the system studied for the case of double BHs by Stegmann & Antonini (2021). However, such amount of mass-loss from the donor is expected to be statistically insignificant for NS + BHs than double BHs.

with $M_{\rm chirp}$) were rejected due to mismatch with $\chi_{\rm rem}$, there were no instances of models accepted/potential match by $\chi_{\rm rem}$ that were rejected due to inconsistency with $\chi_{\rm eff}$.

We also mention here that albeit $M_{\rm chirp}$ and $\chi_{\rm rem}$ are both partial functions of the binary mass ratio, and mass ratio being a more intrinsic binary property, it has high uncertainties observationally. Moreover, for spinning pre-merger BH model (NSBHs, where it may be $\chi_{\rm BH} > 0$) $\chi_{\rm rem}$ no longer solely remains dependant on mass ratio but also on pre-supernovae orbital properties. Similarly, individual masses of the BH and the NS are less constrained than $M_{\rm chirp}$. Hence, we take the observationally more prominent signatures of the binary ($M_{\rm chirp}$ and $\chi_{\rm rem}$) in our comparisons than the intrinsic binary evolution properties (like individual masses or mass ratio).

Stellar metallicity is known to play an important role in the masses of the compact objects, specifically the BHs, through determining wind mass-loss for massive ($\gtrsim$30 $M_\odot$) stars (Vink, de Koter & Lamers 2001; Belczynski et al. 2010; Mapelli et al. 2010). As stellar winds also increase the orbital separation in binaries, the mass transfer history of the binary is also affected by their metallicity. In general, NS + BHs formed at lower metallicity not only tend to be more massive, but their orbital properties, and hence merger time-scales and spin properties also depend on Z.

We evolve 10^6 isolated binaries for each model (Pessimistic, Optimistic, Alpha_2, Kick_100) at each metallicity $Z = 0.0005$, 0.001, 0.005, 0.02, resulting in 16 individual models. We further sub-select systems that merge in 13 Gyr (a Hubble Time, HT) for our analysis as a cut-off, since any system that takes longer to merge will not be a part of the LIGO observations.

We did not account for the redshift evolution of the binaries for the following reasons. The metallicity evolution with redshift is largely uncertain (Furlong et al. 2015; Neijssel et al. 2019), and even the local universe has low metallicity regions (Tramper et al. 2014, 2021). In this paper, we only want to focus on the metallicity environment, rather than its uncertain relationship with redshift evolution. 13 Gyr can be considered an extreme cut-off – any binary taking longer than this time to merge will not be detectable at all. However, the higher Z systems with a shorter merger time may still be observable by the GW detectors. To check this, we varied our cut-off time from 13 to 1 Gyr at an interval of 1 Gyr at every step for the $Z = 0.02$ models. The variation of the median masses and spins were insignificant and none of these changed our conclusions.

To account for GW selection effects favouring more massive binaries, we also weigh the computed chirp mass, effective and remnant spins by the effective volume ($V_{\rm eff} \propto M_{\rm chirp}^{5/2}$) of the binaries, since the GW signal-to-noise ratio depends on the proximity of the merging object to the interferometer, with more massive mergers emitting louder GW signals (as discussed in Chattopadhyay et al. 2020, section 4.2). All further discussions in this paper will only refer to the systems in our data set that merge in an HT, and the median values (including all plots and tables) calculated by $V_{\rm eff}$ weighing, rather than the intrinsic distribution, unless otherwise specified. By using the HT cut-off and biasing the mass and spin distributions by $V_{\rm eff}$ we account for the GW selection effects.

To investigate the spins, each model is post-processed twice under spinning and non-spinning pre-merger BH assumptions (BH-Q and BH-Z). For statistical robustness, we also evolve two test models with same assumptions as Pessimistic and Optimistic. We note that while the test models slightly change the median values, with that for Pessimistic BHNSs always $\lesssim$2.5 per cent and that for their NSBH counterparts as $\lesssim$15 per cent, the highest oscillation being noted for BH-Z $\chi_{\rm eff}$. However, none of these altered our final results and conclusions.

3 RESULTS

For each model, at each metallicity, we use three well-measured observational quantities – the chirp mass ($M_{\rm chirp}$), effective spin ($\chi_{\rm eff}$), and the remnant BH spin ($\chi_{\rm rem}$) of NS + BH systems – and compare them to each of our models. NSBH and BHNS systems are expected to have different mass spectrums (e.g. Chattopadhyay et al. 2021), and the spin distributions of the pre-merger NS and BH of the two types of systems are also different. NSBHs have typically higher spins than BHNSs, since the first born NS can be spun up by accretion from the evolving companion and tidal forces can spin-up the progenitor of the second born BH (for the BH spin model BH-Q). The remnant spins $\chi_{\rm rem}$ are also expected to be distinct between the two sub-populations of NS + BHs, even under the assumption of non-spinning BH model (BH-Z), since the mass ratios of the BHNSs are distinct from the NSBHs (see equation 5). The detailed differences between NSBH and BHNS systems, including their possible observational signatures both through mergers (GWs) as well as pulsars (radio), are discussed in Chattopadhyay et al. (2021). As the mass and spin distributions are different, electromagnetic counterparts of NS + BH mergers such as short gamma-ray bursts can be expected to produce different signatures for the two different sub-populations (Zhu et al. 2021; Sarin et al. 2022). Although, having a non-spinning pre-merger BH, reduces the chances of detecting other electromagnetic counterparts of NS + BH mergers (Barbieri et al. 2020). To further, the mass ratio distribution has a higher uncertainty than $\chi_{\rm rem}$ and for non-spinning BHs ($\chi_{\rm BH} \neq 0$), there is no one-to-one correspondence between mass ratio and remnant spin (see eqations 2 and 6). Thus, $\chi_{\rm rem}$ proves to be a key quantity that reveals the differences between sub-populations, yielding information about the observed system's past and post-merger properties.

To analyse the results, we compare the well-measured observational values of $M_{\rm chirp}$, $\chi_{\rm eff}$, and $\chi_{\rm rem}$ (along with their uncertainty ranges) to the distributions predicted by our models. If the observed values fall within the 10–90th percentile predicted by our model, we declare that the model cannot be ruled out by the data, and is 'accepted'. If the observational values lie beyond the 0.1–100th percentile of the simulated value, we identify the model as 'rejected' for that observation. When an observational data point lies between 0.1th and 10th percentile and 90th and 100th percentile of the computed model, we tag the model as a 'potential match'.

The median value of $M_{\rm chirp}$, $\chi_{\rm eff}$, and $\chi_{\rm rem}$ from the 4 × 4 grid of models (with 4 stellar/binary evolution prescriptions and at 4 metallicities) are presented in Table 1.

We compare the distribution of $M_{\rm chirp}$, $\chi_{\rm rem}$, and $\chi_{\rm eff}$ with the two NS + BH GW observations. The model distributions are shown with the 10th, 50th, and 90th percentiles. These data versus model mass-spin comparison plots are only presented for Pessimistic and Optimistic models. Analysis of the other two pessimistic variations – Kick_100 and Alpha_2 – yields nearly the same final conclusion as Pessimistic, although independent comparisons of the mass or either of the spin measurements may vary.

As mentioned in Section 2, we assume that the spins of the NS and BH prior to merger are aligned with the orbit to calculate $\chi_{\rm eff}$. There are instances in our data set of models accepted by $M_{\rm chirp}$ analysis being rejected by $\chi_{\rm rem}$ (e.g. NSBH at $Z = 0.02$ of model Optimistic for GW200115 as shown in Figs 1 and 3) and vice versa (e.g. NSBH at $Z = 0.001$ of model Optimistic, BH-Z for GW200115 as shown in Figs 1 and 3). It is hence concluded that at least under the aligned spin assumption, $\chi_{\rm rem}$ and $M_{\rm chirp}$ are necessary and sufficient in determining the feasibility of a model. Using only $\chi_{\rm eff}$ and $M_{\rm chirp}$ as pointers may lead to wrong conclusions.

Table 1. The median values of $M_{\rm chirp}$, $\chi_{\rm rem,}$ and $\chi_{\rm eff}$ for the four models Optimistic, Pessimistic, Kick_100, and Alpha_2; each at four metallicities $Z = 0.0005$, 0.001, 0.005, and 0.02, under two pre-merger BH spin assumptions – BH-Q and BH-Z. The standard error (standard deviation/square root of the length of the data set) for all BHNS models remain <0.1 per cent, the pessimistic NSBHs at $Z = 0.02$ has the largest standard error <2 per cent – owing to its smaller data set compared to the rest. This table is used as a reference to compare the observations GW200105 and GW200115 in this paper and may be used similarly for future observations of NS + BH mergers.

Model Name	Metallicity (Z)	$M_{\rm chirp}$ ($M_\odot$) BHNS	NSBH	$\chi_{\rm rem}$ BHNS (BH-Q)	NSBH (BH-Z)	NSBH	$\chi_{\rm eff}$ BHNS (BH-Q)	NSBH (BH-Z)	NSBH
Optimistic	0.0005	3.32	4.30	0.42	0.56	0.20	e−6[a]	0.41	e−6
	0.001	3.65	3.84	0.39	0.59	0.22	e−6	0.44	e−6
	0.005	3.57	3.17	0.36	0.89	0.46	e−6	0.58	e−3
	0.02	2.29	1.92	0.48	0.94	0.66	e−6	0.59	e−6
Pessimistic	0.0005	3.28	2.87	0.44	0.94	0.67	e−6	0.58	e−6
	0.001	3.63	2.71	0.40	0.93	0.68	e−6	0.55	e−6
	0.005	3.58	2.26	0.36	0.94	0.72	e−6	0.52	e−6
	0.02	2.29	2.57	0.49	0.85	0.63	e−6	0.38	e−6
Alpha_2	0.0005	3.07	2.56	0.44	0.97	0.69	e−6	0.62	e−6
	0.001	3.25	2.60	0.42	0.94	0.69	e−6	0.56	e−6
	0.005	3.35	2.13	0.39	0.94	0.72	e−6	0.52	e−6
	0.02	2.04	2.33	0.56	0.75	0.64	e−6	0.24	e−6
Kick_100	0.0005	3.24	2.55	0.45	0.99	0.69	e−6	0.62	e−6
	0.001	3.32	2.55	0.42	0.95	0.69	e−6	0.60	e−6
	0.005	3.46	2.24	0.38	0.99	0.72	e−6	0.58	e−6
	0.02	2.28	2.17	0.51	1.00	0.74	e−6	0.57	e−6

[a] $\chi_{\rm eff}$ $\mathcal{O}(-6)$ can be considered effectively zero.

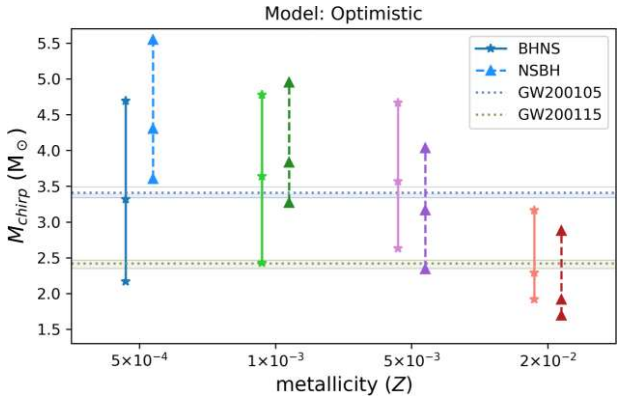

Figure 1. Distribution of chirp masses $M_{\rm chirp}$ of BHNS and NSBH binaries (10th percentile, median and 90th percentile range) as a function of metallicity for model Optimistic. The median values are non-intrinsic, i.e. only consists of systems that merge in a Hubble time, weighted by the effective volume $V_{\rm eff}$. As described in the paper, the sample is obtained for the net population evolved that merges in an HT, weighted by their respective $V_{\rm eff}$ to account for selection biases. The BHNSs are shown with star markers and solid lines, while the NSBHs can be identified by triangle markers and dashed lines. The shaded horizontal lines show the $M_{\rm chirp}$ for GW200105 and GW200115 (Abbott et al. 2021).

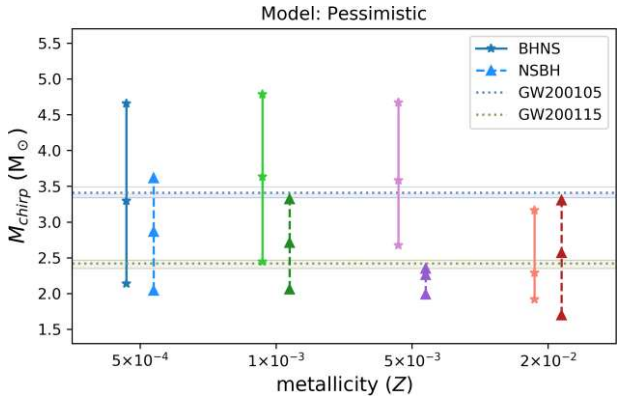

Figure 2. Chirp mass distribution for model Pessimistic with markers identical as that of Fig. 1.

3.1 Chirp mass

The $M_{\rm chirp}$ variation in models Pessimistic and Optimistic is shown in Figs 1 and 2, respectively.

In the model Pessimistic, the BHNS chirp mass median always appear to be slightly larger than NSBHs, while for Optimistic, this gets reversed at lower metallicities. This appears paradoxical, as the dominant formation channels described in Chattopadhyay et al. (2021) for solar metallicity shows the BHs of BHNSs to be more massive – as the more massive star evolves faster and remains more massive enough to form BHs after mass transfer. For NSBHs in this case, the ZAMSs masses of the NS and BH progenitors are nearly equal – where the slightly larger mass star transfers enough mass to its companion to form a NS, whereas the slower evolving companion becomes a BH. However, this formation story changes for lower metallicities. For one, reduced stellar winds ensure the stars lose less mass – creating more massive BHs that would merge in a shorter time-scale than their less massive counterparts (Peters 1964). Secondly, stellar winds may also increase orbital separation. Hence, in metal-poor stars, lower wind loss is also less likely to decrease the orbital separation of the binary – lower orbital separation being crucial for forming NSBHs (as well as BHNSs that merge within an HT). This ensures that while BHNS for model Optimistic at $Z = 0.0005$ form from ZAMS stars with orbital separation roughly 0.53 AU, NSBHs form from binaries with initial separation of about 0.2 of that. The median ZAMSs masses of the two sub-populations NSBH and

BHNSs at Optimistic $Z = 0.0005$ are ($m_{\rm BH}^{\rm ZAMS} = 26.58\,{\rm M}_\odot$, $m_{\rm NS}^{\rm ZAMS} = 32.65\,{\rm M}_\odot$) and ($m_{\rm BH}^{\rm ZAMS} = 33.64\,{\rm M}_\odot$, $m_{\rm NS}^{\rm ZAMS} = 19.19\,{\rm M}_\odot$). At low metallicity, the NSBH progenitor-NS (which remain more massive due to less wind loss), due to close proximity with its companion, starts unstable mass transfer ensuring a CE phase, donating even more mass to its companion. The companion being already massive and also losing less mass for reduced stellar winds, becomes a BH. The BHNSs form from systems with a more unequal mass ratio and larger orbital separation, and an HG donor CE phase is not as essential in its formation as for a NSBH. Hence, we obtain the double compact median masses of NSBHs and BHNSs as $M_{\rm BH} = 20.67\,{\rm M}_\odot$, $M_{\rm NS} = 1.50\,{\rm M}_\odot$ and $M_{\rm BH} = 5.64\,{\rm M}_\odot$, $M_{\rm NS} = 1.56\,{\rm M}_\odot$, respectively. It is indeed interesting to note that the masses of NSBHs are so asymmetric at low metallicity under Optimistic assumption. To compare, we find at $Z = 0.02$, the median masses of the NSBHs and BHNSs are ($M_{\rm BH} = 3.11\,{\rm M}_\odot$, $M_{\rm NS} = 1.46\,{\rm M}_\odot$) and ($M_{\rm BH} = 3.14\,{\rm M}_\odot$, $M_{\rm NS} = 1.37\,{\rm M}_\odot$), respectively. In the Pessimistic scenario, as the HG donor star does not survive the CE, this specific channel – which is dominant for Optimistic NSBHs – is suppressed, and the formation follows the more regular pathway of mass reversal at a higher ZAMS separation. See Broekgaarden et al. (2021a) for more discussion on different NS + BH formation channels and Chattopadhyay et al. (2021) for more discussion on the mass, spin and orbital properties of NS + BH at solar and sub-solar metallicities.

The $M_{\rm chirp}$ of GW200105 is higher than GW200115. For Pessimistic, both GW200105 and GW200115 are in agreement with BHNSs and NSBHs at $Z = 0.0005$, 0.001, while at $Z = 0.005$ GW200105 matches with the BHNS and GW200115 with the NSBH sub-populations. At the higher metallicity of $Z = 0.02$, only the less massive GW200115 can remain consistent with the BHNSs and NSBHs. The metal-rich Pessimistic NSBHs, however, also show a potential match with GW200105. In the Optimistic scenario, GW200105 matches with both BHNS and NSBH systems at $Z = 0.001$, 0.005 and BHNSs at $Z = 0.0005$. NSBHs at $Z = 0.0005$ rests in a potential match zone for GW200105. Only at the very lower limit, does GW200115 match with the BHNSs of Optimistic at $Z = 0.0005$, 0.001, 0.005 and NSBH at $Z = 0.001$. At the high Z end of 0.02, only GW200115 shows good agreement with both BHNSs and NSBHs.

The median $M_{\rm chirp}$ of GW200105 is $3.41\,{\rm M}_\odot$, which matches well with the $M_{\rm chirp}$ of BHNS for all of our models with $Z \leq 0.005$. The less massive GW200115, with an $M_{\rm chirp}$ of about $2.42\,{\rm M}_\odot$, is a better match with the median NSBHs of all three pessimistic group of models at all Z, and with BHNSs of all four models at $Z = 0.02$.

Models Alpha_2 and Kick_100 produces identical consequences in terms of $M_{\rm chirp}$.

3.2 Remnant spin

Figs 3 and 4 show the $\chi_{\rm rem}$ distribution for each metallicity grid under spinning (BH-Q) and non-spinning (BH-Z) assumptions for models Optimistic and Pessimistic, respectively. It is clear that the predictions for NSBHs strongly vary between the BH-Q and BH-Z assumptions. BHNSs always have a non-spinning pre-merger BH and hence have the same $\chi_{\rm rem}$ distribution for both the assumptions.

For Optimistic (Fig. 3), we observe that BHNSs at all metallicities are permissible for both GW200105 and GW200115. BH-Q NSBHs at $Z = 0.0005$ and BH-Z NSBHs at intermediate metallicities $Z = 0.001$, 0.005 also match with both the observations. BH-Q NSBHs at $Z = 0.001$, 0.005 lies on the boundary as potential matches for GW200105.

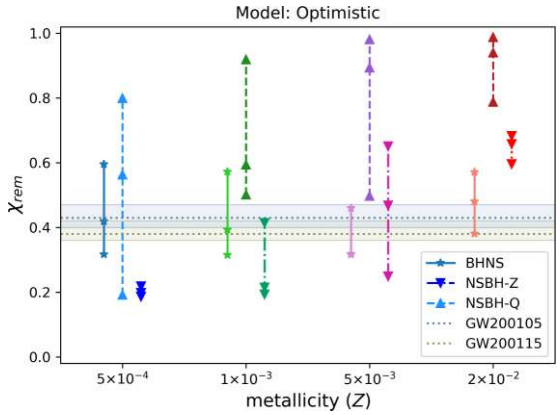

Figure 3. Distribution of the spin of BHNS and NSBH merger remnants $\chi_{\rm rem}$ (at 10th percentile, median and 90th percentile range) as a function of metallicity. The BH-Z NSBHs are plotted with inverted triangles (and dash–dotted lines) and the BH-Q NSBHs are plotted with upright triangles (and dashed lines) as markers. The BHNSs, identical for BH-Q and BH-Z are shown in the symbol of stars (and solid lines). The shaded horizontal regions show the inferred values of GW200105 and GW200115 (Abbott et al. 2021). For additional details, see the main text.

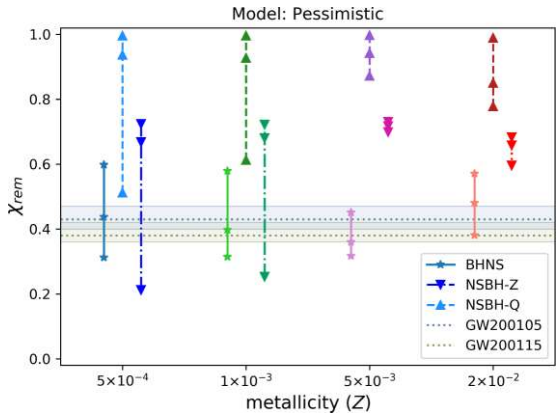

Figure 4. The remnant spin distribution of model Pessimistic at four metallicities. The markers are identical as Fig. 3.

Equations (5) and (6) show that even for non-spinning ($\chi_{\rm BH} = 0$) pre-merger BHs, the remnant BH will be spinning, since the term γ and its coefficients remain non-zero. Even for BH-Z, $\chi_{\rm rem} \gtrsim 0.15$ for Optimistic.

As $M_{\rm BH} > M_{\rm NS}$, more asymmetric mass ratio (effectively, more massive pre-merger BHs) ensure γ is small, making $\chi_{\rm rem}$ small. As described in Section. 3.1, metal-poor NSBHs have fairly massive BHs. This, with the BH-Z assumption, makes NSBH $\chi_{\rm rem}$ at $Z = 0.0005$, 0.001 of Optimistic quite modest. For BH-Q, even with highly asymmetric mass ratio, these low metallicity NSBHs show median $\chi_{\rm rem} \approx 0.55$. Guided by equation (2), small orbital separation (and hence shorter period $p_{\rm orb}$) between the two stars in these systems (as discussed in Section. 3.1) aids in producing higher $\chi_{\rm BH}$.

In the model Pessimistic (Fig. 4), BHNSs at all metallicities match with both of the GW observations. Even with large median values of $\chi_{\rm rem}$, BH-Z NSBHs at $Z = 0.0005$, 0.001 are consistent with GW200105 and GW200115. The only difference between Pessimistic and Kick_100, Alpha_2 is observed for $Z = 0.02$ $\chi_{\rm rem}$ for BHNSs. While for Pessimistic, this is permissible for GW200115, both Kick_100 and Alpha_2 discludes these variations.

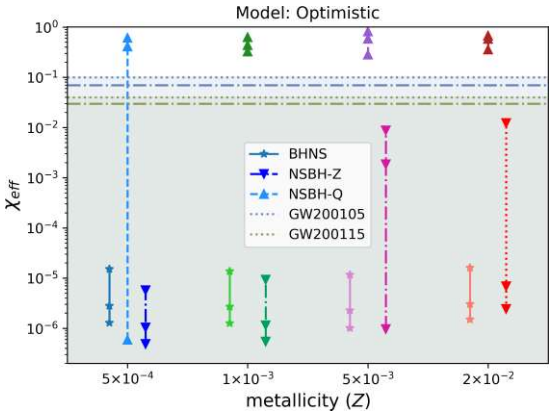

Figure 5. Effective spin distribution of model Optimistic with markers identical to Fig. 3. The horizontal lines in blue and green show the upper limits of $\chi_{\rm eff}$ observations of GW200105 and GW200115, respectively. Of these horizontal lines, the dotted and dash–dotted lines are the upper limits for a higher and lower spin priors, respectively. Since we only assume aligned spin model, we show the part of observations (shaded region), where $\chi_{\rm eff} > 0$.

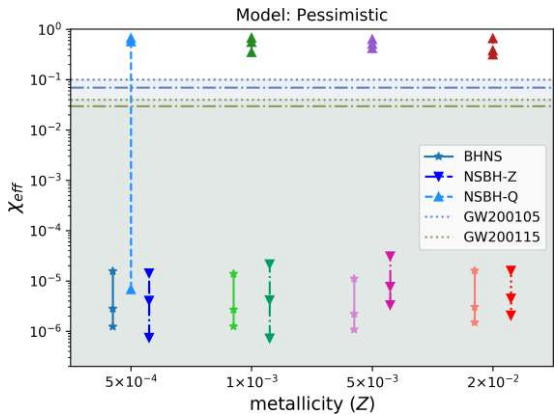

Figure 6. Effective spin distribution for model Pessimistic with identical symbols as Fig. 5.

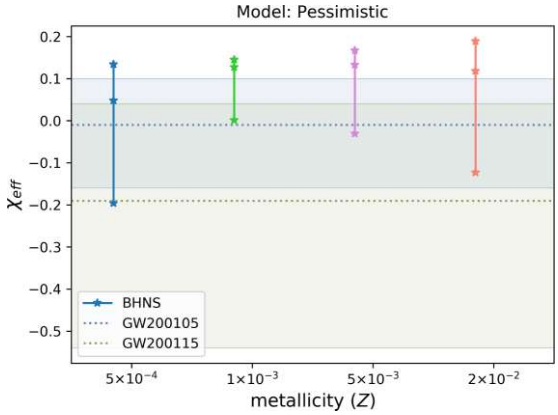

Figure 7. Effective spin distribution for model PessimisticST, showing the BHNSs. The shaded region for GW200105 and GW200115 are as inferred by Abbott et al. (2021), under high secondary spin prior. We note that although spin misalignment allows for negative $\chi_{\rm eff}$, the median of all distributions are greater than 0.

Solely observing the $\chi_{\rm rem}$ medians in Table. 1, and comparing that with the observations of GW200105 and GW200115 with remnant spins of about 0.43 and 0.38, respectively, we see that apart from metal-poor Optimistic models, all other models with BH-Q spin assumptions have quite large $\chi_{\rm rem}$ medians. All BHNSs in models with $Z \leq 0.005$ match fairly well with the two observations. However, BH-Z NSBHs, though still having higher median, show some matches (see Figs 3 and 4).

We also check the $\chi_{\rm rem}$ PessimisticST model, replacing $\chi_{\rm BH}$ of eqation (6) with $\chi_{\rm BH}\cos\theta$ (where θ is the spin misalignment angle of the pre-merger BH with the orbital angular momentum). The computed $\chi_{\rm rem}$ does not alter our conclusions, only bringing the NSBH-Q to slightly ($<$0.1) lower values, making $Z = 0.0005$ NSBH-Q $\chi_{\rm rem}$ a plausible model for both GW200105 and GW200115 for its $10^{\rm th}$ percentile boundary (the median value $\approx$0.75 still remains well above the observations). Since the first born BH of the BHNSs are always assumed non-spinning, we further compute a special variation of this population with the magnitude of the first born BH spin $\chi_{\rm BH} = 0.1$, making $\chi_{\rm BH}\cos\theta$ non-zero for BHNSs. Still, this does not alter our conclusions and the $\chi_{\rm rem}$ distribution is very slightly adjusted to smaller values.[5]

3.3 Effective spin

Although we have described that $M_{\rm chirp}$ and $\chi_{\rm rem}$ are together sufficient in constraining our models, we show the distribution of $\chi_{\rm eff}$ for models Optimistic and Pessimistic (for both spin models BH-Q and BH-Z) in Figs 5 and 6, respectively.

We note here that for $\chi_{\rm eff}$, both Optimistic and Pessimistic (and hence all four models) lead to identical conclusions. We observe that BHNSs at all of the metallicities modelled, as well as all NSBHs with BH-Z assumption and metal poor ($Z = 0.0005$) BH-Q NSBHs are congruent with both the GW mergers. The large uncertainty of $\chi_{\rm eff}$ indeed puts poor constraints for the models.

The primary contribution to $\chi_{\rm eff}$ comes from the spin of the BH, owing to its higher mass than the NS (see equation 4). Hence, fast spinning BHs of BH-Q can impart NSBHs with much higher $\chi_{\rm eff}$ than BHNS. For BH-Z on the other hand, NSBHs consisting of very massive, non-spinning BHs tend to have larger denominators in equation (4), resulting in small $\chi_{\rm eff}$ values (as seen in Optimistic BH-Z NSBHs at $Z = 0.0005, 0.001$). The PessimisticST model that allows for spin misalignment is still shown to be biased towards zero or positive $\chi_{\rm eff}$, allowing negative values only in a minority of the systems. We note that PessimisticST again, does not alter our conclusions (see Fig. 7).

3.4 Constraints from mass and spin

Using the analysis of Sections 3.1, 3.2, and 3.3, we produce the following conclusions from each of the four models in Table 2. The summary of Table 2 is given here:

(i) Optimistic:
GW200105 – *accepted* for BHNS at $Z = 0.0005, 0.001, 0.005$, NSBH BH-Z at $Z = 0.001, 0.005$; *potential match* for NSBH BH-Q at $Z = 0.0005, 0.001, 0.005$, NSBH BH-Z at $Z = 0.0005$; *rejected* for BHNS or NSBH at $Z - 0.02$.

[5]It allows $Z = 0.0005$ BHNS to have the 10th percentile of $\chi_{\rm rem} = -0.001$, but all changes for other models are unremarkable. We, hence, see that at low metallicity, anti-aligned merger remnant is possible due to pre-merger BH orbital misalignment, but the magnitude of the $\chi_{\rm rem}$ still remains very close to zero.

Table 2. The grid of models and their match with the two NS + BH merger observations through mass and spin analysis. The models that are *accepted* are denoted by 'gw05' or 'gw15' for GW200105 or GW200115, respectively. The *potential match* models are identified by a dagger (†) symbol and the *rejected* ones are dashed (–).

Model		Results		
Name	Metallicity (Z)	NSBH		BHNS
–	–	(BH-Q)	(BH-Z)	
Optimistic	0.0005	gw05†	–	gw05, gw15
	0.001	gw05†	gw05	gw05, gw15
	0.005	gw05†	gw05, gw15	gw05
	0.02	–	–	gw15
Pessimistic	0.0005	–	gw05, gw15	gw05, gw15
	0.001	–	gw05†, gw15	gw05, gw15
	0.005	–	–	gw05, gw15
	0.02	–	–	gw15
Alpha_2	0.0005	–	gw05, gw15	gw05, gw15
	0.001	–	gw05†, gw15	gw05, gw15
	0.005	–	–	gw05, gw15
	0.02	–	–	–
Kick_100	0.0005	–	gw05, gw15	gw05, gw15
	0.001	–	gw05†, gw15	gw05, gw15
	0.005	–	–	gw05, gw15
	0.02	–	–	–

GW200115 – *accepted* for BHNS at $Z = 0.0005$, 0.001, BHNS at $Z = 0.02$, NSBH BH-Z at $Z = 0.005$; *rejected* for BHNS at $Z = 0.005$.

(ii) Pessimistic, Alpha_2, Kick_100:
GW200105 – *accepted* for BHNS at $Z = 0.0005, 0.001, 0.005$, NSBH BH-Z at $Z = 0.0005$; *potential match* for NSBH BH-Z at $Z = 0.001$.
GW200115 – *accepted* for BHNS at $Z = 0.0005, 0.001, 0.005$, NSBH BH-Z at $Z = 0.0005$, 0.001. GW200115 is *accepted* for BHNS at $Z = 0.02$ for Pessimistic, *rejected* for Alpha_2, Kick_100.
It is to be noted that only Alpha_2 and Kick_100 are the models that matches with the results of Broekgaarden & Berger (2021).

We note that the qualitative conclusions from the Optimistic and Pessimistic models are not vastly different from each other. Sub-solar metallicity and BHNSs are preferred. For Alpha_2 and Kick_100, no $Z = 0.02$ population are consistent with the two GW observations. Only with GW200115 does metal-rich $Z = 0.02$ Optimistic BHNSs show a consistency. The NSBHs that are in agreement with observations for all four models are for non-spinning pre-merger BH (i.e. spin model BH-Z). Only for Optimistic does GW200105 shows a potential matching with BH-Q NSBHs.

Emphasizing the median values of Table 1, $Z \lesssim 0.005$ BHNSs show a better match of $M_{\rm chirp}$ and $\chi_{\rm rem}$ of GW200105. The less massive GW200115 fits better with metal-rich values of $M_{\rm chirp}$ for BHNSs of all models, and all NSBHs values of the pessimistic group of models. The $\chi_{\rm rem}$ medians of NSBHs are, however, too high for GW200115 NSBHs (especially BH-Q models). This makes either a metal-rich BHNS or BH-Z NSBH a more likely source of GW200115.

3.5 Relative merger rate

The relative merger rates of NS + BH systems are presented in Table 3, which only accounts for the systems that merges in an HT. The column $\mathcal{R}_{\rm NSBH/BHNS}$ shows the ratio of merging NSBHs to merging BHNSs in each model. While all models produce more BHNSs, Optimistic $Z = 0.001$ produces the largest fraction of

Table 3. The relative merger rates of NS + BH systems for our grid of models, where $\mathcal{R}_{\rm NSBH/BHNS}$ = NSBH/BHNS that merges in an HT for that model and $\mathcal{R}_{\rm norm.BHNS}$ = BHNS/(BHNS, Optimistic, Z = 0.0005) that merges in an HT.

Model		Rates	
Name	Metallicity (Z)	$\mathcal{R}_{\rm NSBH/BHNS}$	$\mathcal{R}_{\rm norm.BHNS}$
Optimistic	0.0005	1.79e−1	1
	0.001	2.91e−1	1.07
	0.005	1.94e−1	2.17
	0.02	6.89e−2	0.43
Pessimistic	0.0005	6.37e−2	0.88
	0.001	9.59e−2	0.94
	0.005	5.59e−3	1.99
	0.02	3.77e−3	0.29
Alpha_2	0.0005	9.00e−2	2.59
	0.001	8.89e−2	2.30
	0.005	3.23e−2	3.10
	0.02	3.84e−3	0.34
Kick_100	0.0005	9.94e−2	2.29
	0.001	0.57e−2	2.37
	0.005	9.91e−3	4.71
	0.02	9.88e−4	1.64

NSBHs. The column $\mathcal{R}_{\rm norm.BHNS}$ marks the merging BHNSs in each model normalized by the merging BHNSs in Optimistic $Z = 0.0005$. We observe that Kick_100 at $Z = 0.005$ has the most BHNSs. It is further noted that since BHNS dominates the population significantly at all metallicities – hence non-spinning pre-merger BHs being more common – the chances of having an electromagnetic counterpart for NS + BH mergers is rare (Barbieri et al. 2020; Hu et al. 2022). For the cosmological merger rates, we refer to Broekgaarden et al. (2021a), Broekgaarden & Berger (2021). We note that the cosmological rates are in agreement with our model, but large uncertainties in predictions (Neijssel et al. 2019; Broekgaarden & Berger 2021). The LIGO/Virgo inferred local merger rate medians vary (12–242 $\rm Gpc^{-3}\,yr^{-1}$) depending on assumptions made about the distribution of the individual component masses, and have broad lower/upper limits (Abbott et al. 2021).

4 CONCLUSIONS

We analysed the first two observations of NS + BH systems by LIGO/Virgo (Abbott et al. 2021) using the rapid binary population synthesis code COMPAS (Stevenson et al. 2017; Vigna-Gómez et al. 2018). We compared these observations to four different models with various different assumptions regarding poorly constrained stages of massive binary evolution (the CE phase and natal kicks obtained in supernovae). For each model, we examined how the properties of NS + BH vary with metallicity, using a grid of four different metallicities ($Z = 0.0005$, 0.001, 0.005, 0.02). We used several well-measured observables (the binary chirp mass, the effective spin and the spin of the remnant BH) as constraints on our models and showed that under the assumption of aligned spins, the observations are well in agreement with isolated binary evolution.

The observational data for GW200115 shows possible evidence for significant spin-orbit misalignment (Abbott et al. 2021). Several authors have argued that high natal kicks would be necessary to mis-align the spin to such a high degree (Fragione, Loeb & Rasio 2021; Zhu 2021; Gompertz et al. 2022). However, Broekgaarden & Berger (2021) showed smaller supernova kicks provide a better match

with observations once the rates of all compact object mergers are taken into account. Moreover, it has been shown that the spin alignment results of the double BH observations are quite prior-dependant (Galaudage et al. 2021), and even for the two NS + BH mergers, a different choice yields non-spinning pre-merger BHs, not requiring any misalignment (Mandel & Smith 2021). We show by model PessimisticST that although misalignment by supernovae kick may explain the negative $\chi_{\rm eff}$, the dominant population still have aligned, nearly zero BH spins. We assumed aligned spins for pre-merger BHs. The BH spins are computed in two models of spinning BH-Q (Qin et al. 2018) and non-spinning BH-Z. The NS spin, used for calculating the effective spin, is also modelled in detail (Chattopadhyay et al. 2020, 2021). The remnant spin of the post-merger BH is calculated using fits from Zappa et al. (2019) at different metallicities.

The answers to our questions at the beginning (Section 1) can be consolidated from Section 3.4 as

(a) Making use of multiple well-measured observables, such as $M_{\rm chirp}$ and $\chi_{\rm rem}$ does indeed aid in distinguishing qualitatively between two sub-populations (NSBH versus BHNS). Both observations are in favour of BHNSs, as well as a few matches for NSBHs (Section 3.4).

(b) In our models, we find that systems in which the NS forms first (NSBHs) typically contribute $\lesssim$1 per cent of merging NS + BH binaries, though it varies from model to model, the range being $\sim$0.1−30 per cent (Table 3). This significantly shifts the quantitative analysis in favour of BHNSs, especially for the pessimistic group of models. The relative merger rates of the two sub-populations BHNSs and NSBHs, as well as the relative merger rates of BHNSs in our 16 models is presented in Table 3. Although there are more matches with BHNSs at different metallicities for both models, with non-spinning pre-merger BH model (BH-Z), NSBHs are also in agreement with the observations.

(c) Our models show that a non-spinning BH (prior to merger) is highly preferred for both GW200105 and GW200115 (see also Mandel & Smith 2021). There is only one *potential match* for a pre-merger spinning BH for GW200105 with model Optimistic. All three pessimistic models – Pessimistic, Alpha_2, and Kick_100 have only non-spinning model as *accepted*.

(d) In our analysis, we find that the effective spin parameter $\chi_{\rm eff}$ does not add any extra constraints on our models.

(e) Formation in a sub-solar metallicity environment ($Z \lesssim 0.005$ is strongly preferred for both GW200105 and GW200115, coming from analysing the $\chi_{\rm rem}$ of Kick_100 and Alpha_2. However, GW200115 does match with only two metal-rich models ($Z = 0.02$, Optimistic, Pessimistic).

We further note that $\chi_{\rm rem}$, being a well-measured parameter (than, say, mass-ratio), can be utilized to differentiate between the sub-populations BHNSs and NSBHs (BH-Q and BH-Z).

Further, the paucity of NSBHs compared to BHNSs by several orders of magnitude and the general favouring of non-spinning BH models reveals that electromagnetic counterparts to NS + BH mergers are likely quite infrequent.

Our results are solely valid for isolated binary evolution. It is also helpful to bear in mind here, that the expected merger rate of NS + BH systems through the dynamical channel of young star clusters is found plausible in some studies (Rastello et al. 2020), but others find this type of binary merger to be quite low for nuclear, globular, as well as young clusters (Clausen, Sigurdsson & Chernoff 2013; Petrovich & Antonini 2017; Fragione & Banerjee 2020). The uncertainties of initial conditions (e.g. mass ratio and orbital period distributions) and binary evolution processes (e.g. CE, supernovae kicks, post-supernova core mass to compact object mass mapping) also adds to the complexities (Stevenson et al. 2017; Vigna-Gómez et al. 2018; Broekgaarden et al. 2021a; Chattopadhyay et al. 2021). While we did vary some of these parameters of massive binary evolution, others were kept constant. The models selected for this study were primarily guided by the models already short listed by Broekgaarden & Berger (2021) based on the chirp mass of the two NS + BH mergers and the merger rates of all types of observed LIGO/Virgo mergers from the first two observing runs (Alpha_2 and Kick_100). Two other models Pessimistic and Optimistic were also added to follow the effect of this change in parameters on our results. We acknowledge that while a portion of the partially constrained massive binary parameter space has been explored by our models, there still remains further uncertainties such as mass transfer efficiency, pre-supernova core mass to remnant mass models or different wind prescriptions (Broekgaarden et al. 2021b). While exploring the entirety of this parameter space is beyond the scope of this study, more compact binary observations (having better signal-to-noise ratio that detects the masses and spins with better precision) will aid in restricting the uncertainties.

We observed that all four models gave nearly identical conclusions, with Optimistic varying the most. Hence, while CE prescription does appear to affect the results, other variations within the limitations imposed by merger rates do not appear to dramatically alter our conclusions.

Future possible observations of more NS + BH mergers by LIGO/Virgo/KAGRA (Belczynski et al. 2016; Mapelli & Giacobbo 2018; Broekgaarden et al. 2021b), NS + BH binaries by LISA (Chattopadhyay et al. 2021; Wagg et al. 2021) or even pulsars in binaries with BHs by radio telescopes like the SKA (Kyutoku, Nishino & Seto 2019; Chattopadhyay et al. 2021) will aid in shedding more light on the mass and spin distribution of these systems and hence put better constraints on massive binary evolution. Moreover, with more observations in GWs as well as possible observations as radio pulsars of NS + BH systems, there will be higher scopes of differentiating the two NSBH and BHNS sub-populations. Table 1 showing the medians of mass and spin from our different models and sub-populations can be used as a comparative grid for future observations of NS + BH coalescence(s).

ACKNOWLEDGEMENTS

We thank Jarrod Hurley for the useful insights and discussions. DC thanks Michela Mapelli for her comments. We are grateful to the journal referee for their suggestions. DC and SS were supported by the Australian Research Council (ARC) Centre of Excellence for Gravitational Wave Discovery (OzGrav), through project number CE170100004. DC was supported by the STFC grant ST/V005618/1. FA was supported by an STFC Rutherford fellowship (ST/P00492X/2). SS is a recipient of an ARC Discovery Early Career Research Award (DE220100241). This work made use of the OzSTAR high-performance computer at Swinburne University of Technology. OzSTAR is funded by Swinburne University of Technology and the National Collaborative Research Infrastructure Strategy (NCRIS).

DATA AVAILABILITY

Simulations in this paper made use of the COMPAS rapid binary population synthesis code, which is freely available at http://github.com/TeamCOMPAS/COMPAS (Stevenson et al. 2017;

Vigna-Gómez et al. 2018; Team COMPAS et al. 2022). The simulations performed in this work were simulated with a COMPAS version that predates the publicly available code. Our version of the code is most similar to version 02.13.01 of the publicly available COMPAS code. Requests for the original code can be made to the lead author.

REFERENCES

Aasi J. et al., 2015, Class. Quantum Gravity, 32, 074001
Abbott R. et al., 2021, ApJ, 915, L5
Acernese F. et al., 2015, Class. Quantum Gravity, 32, 024001
Asplund M., Grevesse N., Sauval A. J., Scott P., 2009, ARA&A, 47, 481
Barbieri C., Salafia O. S., Perego A., Colpi M., Ghirlanda G., 2020, Eur. Phys. J. A, 56, 8
Bavera S. S. et al., 2020, A&A, 635, A97
Belczynski K., Taam R. E., Kalogera V., Rasio F. A., Bulik T., 2007, ApJ, 662, 504
Belczynski K., Kalogera V., Rasio F. A., Taam R. E., Zezas A., Bulik T., Maccarone T. J., Ivanova N., 2008, ApJS, 174, 223
Belczynski K., Bulik T., Fryer C. L., Ruiter A., Valsecchi F., Vink J. S., Hurley J. R., 2010, ApJ, 714, 1217
Belczynski K., Repetto S., Holz D. E., O'Shaughnessy R., Bulik T., Berti E., Fryer C., Dominik M., 2016, ApJ, 819, 108
Belczynski K. et al., 2022, ApJ, 925, 69
Broekgaarden F. S., Berger E., 2021, ApJ, 920, L13
Broekgaarden F. S. et al., 2021a, MNRAS, 508, 5028
Broekgaarden F. S. et al., 2021b, preprint (arXiv:2112.05763)
Chattopadhyay D., Stevenson S., Hurley J. R., Rossi L. J., Flynn C., 2020, MNRAS, 494, 1587
Chattopadhyay D., Stevenson S., Hurley J. R., Bailes M., Broekgaarden F., 2021, MNRAS, 504, 3682
Clausen D., Sigurdsson S., Chernoff D. F., 2013, MNRAS, 428, 3618
Clausen D., Sigurdsson S., Chernoff D. F., 2014, MNRAS, 442, 207
Cutler C. et al., 1993, Phys. Rev. Lett., 70, 2984
Damour T., Nagar A., 2010, Phys. Rev. D, 81, 084016
de Mink S. E., Belczynski K., 2015, ApJ, 814, 58
Foucart F., 2020, Front. Astron. Space Sci., 7, 46
Fragione G., Banerjee S., 2020, ApJ, 901, L16
Fragione G., Loeb A., Rasio F. A., 2021, ApJ, 918, L38
Fryer C. L., Belczynski K., Wiktorowicz G., Dominik M., Kalogera V., Holz D. E., 2012, ApJ, 749, 91
Fuller J., Ma L., 2019, ApJ, 881, L1
Furlong M. et al., 2015, MNRAS, 450, 4486
Galaudage S., Talbot C., Nagar T., Jain D., Thrane E., Mandel I., 2021, ApJ, 921, L15
Gessner A., Janka H.-T., 2018, ApJ, 865, 61
Giacobbo N., Mapelli M., Spera M., 2018, MNRAS, 474, 2959
Gompertz B. P., Nicholl M., Schmidt P., Pratten G., Vecchio A., 2022, MNRAS, 511, 1454
Hinderer T., Lackey B. D., Lang R. N., Read J. S., 2010, Phys. Rev. D, 81, 123016
Hobbs G., Lorimer D. R., Lyne A. G., Kramer M., 2005, MNRAS, 360, 974
Hu R.-C., Zhu J.-P., Qin Y., Zhang B., Liang E.-W., Shao Y., 2022, ApJ, 928, 163
Hurley J. R., Pols O. R., Tout C. A., 2000, MNRAS, 315, 543
Hurley J. R., Tout C. A., Pols O. R., 2002, MNRAS, 329, 897
Klencki J., Moe M., Gladysz W., Chruslinska M., Holz D. E., Belczynski K., 2018, A&A, 619, A77
Kochanek C. S., 1992, ApJ, 398, 234
Kroupa P., 2001, MNRAS, 322, 231
Kyutoku K., Nishino Y., Seto N., 2019, MNRAS, 483, 2615
Lattimer J. M., Schramm D. N., 1976, ApJ, 210, 549
MacLeod M., Ramirez-Ruiz E., 2015, ApJ, 798, L19
Mandel I., Smith R. J. E., 2021, ApJ, 922, L14
Mapelli M., Giacobbo N., 2018, MNRAS, 479, 4391
Mapelli M., Ripamonti E., Zampieri L., Colpi M., Bressan A., 2010, MNRAS, 408, 234
Müller B. et al., 2019, MNRAS, 484, 3307
Neijssel C. J. et al., 2019, MNRAS, 490, 3740
Olejak A., Belczynski K., Ivanova N., 2021, A&A, 651, A100
Peters P. C., 1964, Phys. Rev., 136, 1224
Petrovich C., Antonini F., 2017, ApJ, 846, 146
Podsiadlowski P., Langer N., Poelarends A. J. T., Rappaport S., Heger A., Pfahl E., 2004, ApJ, 612, 1044
Qin Y., Fragos T., Meynet G., Andrews J., Sørensen M., Song H. F., 2018, A&A, 616, A28
Rastello S., Mapelli M., Di Carlo U. N., Giacobbo N., Santoliquido F., Spera M., Ballone A., Iorio G., 2020, MNRAS, 497, 1563
Sana H. et al., 2012, Science, 337, 444
Sarin N., Lasky P. D., Vivanco F. H., Stevenson S. P., Chattopadhyay D., Smith R., Thrane E., 2022, Phys. Rev. D, 105, 083004
Schneider F. R. N., Izzard R. G., Langer N., de Mink S. E., 2015, ApJ, 805, 20
Sharda P., Krumholz M. R., Wisnioski E., Acharyya A., Federrath C., Forbes J. C., 2021, MNRAS, 504, 53
Sigurdsson S., 2003, in Bailes M., Nice D. J., Thorsett. S. E., eds, ASP Conf. Ser. Vol. 302, Black Holes and Pulsar Binaries. Astron. Soc. Pac., San Francisco, p. 391
Stegmann J., Antonini F., 2021, Phys. Rev. D, 103, 063007
Stevenson S., Vigna-Gómez A., Mandel I., Barrett J. W., Neijssel C. J., Perkins D., de Mink S. E., 2017, Nat. Commun., 8, 14906
Team COMPAS et al., 2022, ApJS, 258, 34
The LIGO Scientific Collaboration, the Virgo Collaboration, the KAGRA Collaboration, 2021, preprint (arXiv:2111.03634)
Tramper F., Sana H., de Koter A., Kaper L., Ramírez-Agudelo O. H., 2014, A&A, 572, A36
Vigna-Gómez A. et al., 2018, MNRAS, 481, 4009
Vink J. S., de Koter A., Lamers H. J. G. L. M., 2001, A&A, 369, 574
Wagg T., Broekgaarden F. S., de Mink S. E., van Son L. A. C., Frankel N., Justham S., 2021, preprint (arXiv:2111.13704)
Xu X.-J., Li X.-D., 2010, ApJ, 716, 114
Zappa F., Bernuzzi S., Pannarale F., Mapelli M., Giacobbo N., 2019, Phys. Rev. Lett., 123, 041102
Zhu X.-J., 2021, ApJ, 920, L20
Zhu J.-P., Wu S., Yang Y.-P., Zhang B., Yu Y.-W., Gao H., Cao Z., Liu L.-D., 2021, ApJ, 921, 156

This paper has been typeset from a TEX/LATEX file prepared by the author.